FINAL TECHNICAL REPORT FOR THE US DEPARTMENT OF ENERGY

Project title: Metal-organic and zeolitic imidazolate frameworks (MOFs and ZIFs) for highly selective separations
Covering Period: 02/01/2008 to 01/31/2012
Recipient: Center for Reticular Chemistry, Department of Chemistry and Biochemistry, University of California - Los Angeles
Award number: DE-FG02-08ER15935
Project director: Omar M. Yaghi
Contact: 607 Charles E. Young Drive East, Los Angeles, CA 90095
Phone: (310) 206-0398; Fax: (310) 206-5891
E-mail: yaghi@chem.ucla.edu

Executive Summary

Metal-organic and zeolite imidazolate frameworks (MOFs and ZIFs) have been investigated for the realization as separation media with high selectivity. These structures are held together with strong bonds, making them architecturally, chemically, and thermally stable. Therefore, employing well designed building units, it is possible to discover promising materials for gas and vapor separation. This grant was focused on the study of MOFs and ZIFs with these specific objectives: (i) to develop a strategy for producing MOFs and ZIFs that combine high surface areas with active sites for their use in gas adsorption and separation of small organic compounds, (ii) to introduce active sites in the framework by a post-synthetic modification and metalation of MOFs and ZIFs, and (iii) to design and synthesize MOFs with extremely high surface areas and large pore volumes to accommodate large amounts of guest molecules.

By the systematic study, this effort demonstrated how to introduce active functional groups in the frameworks, and this is also the origin of a new strategy, which is termed isoreticular functionalization and metalation. However, a large pore volume is still a prerequisite feature. One of the solutions to overcome this challenge is an isoreticular expansion of a MOF's structure. With triangular organic linker and square building units, we demonstrated that MOF-399 has a unit cell volume 17 times larger than that of the first reported material isoreticular to it, and it has the highest porosity (94%) and lowest density (0.126 g cm^{-3}) of any MOF reported to date. MOFs are not just low density materials; the guest-free form of MOF-210 demonstrates an ultrahigh porosity, whose BET surface area was estimated to be 6240 m^2 g^{-1} by N_2 adsorption measurements.

This report does not contain any proprietary, confidential,
or otherwise restricted information.

Executive Summary

Metal-organic and zeolite imidazolate frameworks (MOFs and ZIFs) have been investigated for the realization as separation media with high selectivity. These structures are held together with strong bonds, making them architecturally, chemically, and thermally stable. Therefore, employing well designed building units, it is possible to discover promising materials for gas and vapor separation. This grant was focused on the study of MOFs and ZIFs with these specific objectives: (i) to develop a strategy for producing MOFs and ZIFs that combine high surface areas with active sites for their use in gas adsorption and separation of small organic compounds, (ii) to introduce active sites in the framework by a post-synthetic modification and metalation of MOFs and ZIFs, and (iii) to design and synthesize MOFs with extremely high surface areas and large pore volumes to accommodate large amounts of guest molecules.

By the systematic study, this effort demonstrated how to introduce active functional groups in the frameworks, and this is also the origin of a new strategy, which is termed isoreticular functionalization and metalation. However, a large pore volume is still a prerequisite feature. One of the solutions to overcome this challenge is an isoreticular expansion of a MOF's structure. With triangular organic linker and square building units, we demonstrated that MOF-399 has a unit cell volume 17 times larger than that of the first reported material isoreticular to it, and it has the highest porosity (94%) and lowest density (0.126 g cm^{-3}) of any MOF reported to date. MOFs are not just low density materials; the guest-free form of MOF-210 demonstrates an ultrahigh porosity, whose BET surface area was estimated to be 6240 m^2 g^{-1} by N_2 adsorption measurements.

Project Objective

The proposed program was focused on further developing metal-organic frameworks (MOFs) in separation technologies. A new class of materials named zeolite imidazolate frameworks (ZIFs), which were recently invented in our laboratory, was studied for their high selective gas adsorption behaviors. More specifically we have undertaken our efforts:

- To develop strategies to incorporate active sites in MOFs and ZIFs
- To develop chemistry for isoreticular modification and metalation of the crystalline porous solids
- To utilize new concepts for increased surface area and pore volume.

Background

MOFs and ZIFs have recently emerged as an important class of porous materials for their amenability to design and the flexibility with which their pores can be functionalized. In particular, their extraordinary low density (1.00 to 0.20 g/cm^3), high surface areas (> 3000 m^2/g), and the remarkable chemical and thermal stability of ZIFs in particular make them ideal candidates for the storage and separation of gases. Previous work has developed the synthetic protocol for producing crystalline ZIFs. Using this method we made a dozen structures of various topologies and tested their stability and porosity.

Results

1. Colossal cages in ZIFs for gas capture

ZIFs are porous crystalline materials with tetrahedral networks that resemble those of zeolites [1-4]: transition metals (Zn, Co) replace tetrahedrally coordinated atoms (for example, Si), and imidazolate links replace oxygen bridges. A striking feature of these materials is that the structure adopted by a given ZIF is determined by link-link interactions, rather than by the structure directing agents used in zeolite synthesis. As a result, systematic variations of linker substituents have yielded many different ZIFs that exhibit known or predicted zeolite topologies. Here we synthesized two new ZIFs and characterized and their potential applications in selective carbon dioxide capture was analyzed [5].

ZIF-95 ($Zn(cbIm)_2$, where cbIm is 5-chlorobenzimidazole, Figure 1) was synthesized by heating a solution mixture of cbIm and $Zn(NO_3)_2 \cdot 4H_2O$ in H_2O/*N*,*N*-dimethylformamide (DMF) at 120 °C for 72 h to give light yellow plate crystals. Restricting the water content of the reaction medium used for ZIF-95 synthesis promotes the crystallization of a new phase, ZIF-100 ($Zn_{20}(cbIm)_{39}(OH)$). Less hydrated conditions (anhydrous DMF) are achieved by using anhydrous $Zn(O_3SCF_3)_2$ in place of $Zn(NO_3)_2 \cdot 4H_2O$. The structural features of these ZIFs uniquely combines huge cavities (24.0 Å and 35.6 Å for ZIF-95 and 100, respectively) and highly constricted windows (largest aperture, 3.65 Å and 3.35 Å); this aspect that pointed to their possible utility in carbon dioxide capture and storage Figure 1.

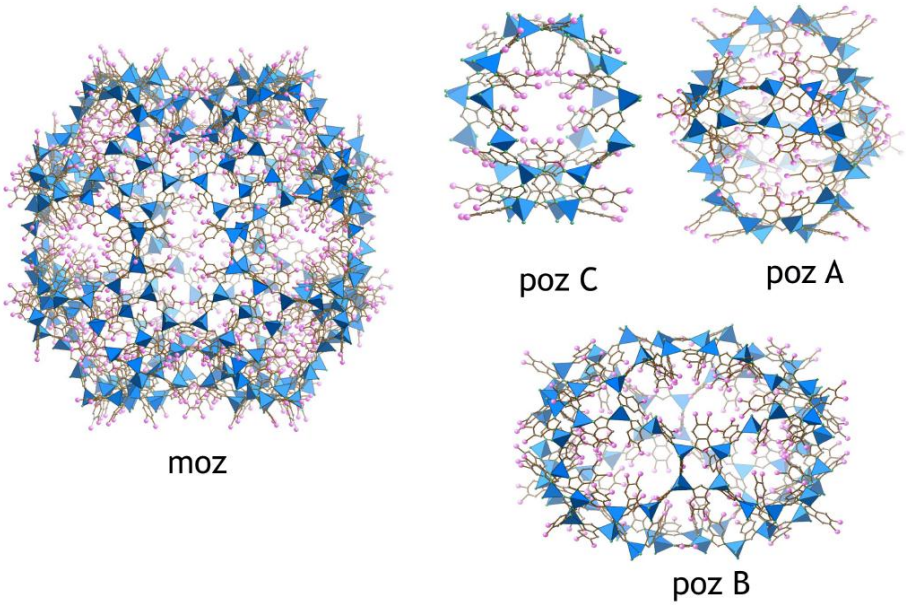

Figure 1. Pore cages of ZIF-100 (moz) and ZIF-95 (poz C, poz B, Poz A).

Their permanent porosity was proven using a N_2 or Ar adsorption measurement. The Langmuir (BET) surface areas were 1,240 (1050) $m^2\ g^{-1}$ and 780 (595) $m^2\ g^{-1}$ for ZIF-95 and ZIF-100, respectively (Figure 2a), which is more than double those of the most porous zeolites. CO_2, CH_4, CO and N_2 adsorption isotherms were measured for both ZIFs at 298 K (Figure 2b), and clearly show a disproportionately high affinity and capacity for CO_2. ZIF-100 is seen to outperform ZIF-95 and the prototypical adsorbent BPL carbon [6]. Both ZIFs show complete

reversibility of CO_2 adsorption isotherms, thus indicating their potential as selective CO_2 reservoirs to hold CO_2. More detailed analysis of the data in Figure 2b indicates that one liter of ZIF-100 can hold up to 28.2 L (55.4 g, or 1.7 mmol per one gram of ZIF-100) of CO_2 at 273 K and 15.9 L (31.2 g) at 298 K. The Henry's Law constant, derived from the initial slope of the Toth model was used to calculate the gas selectivity on ZIFs. As indicated in Table 1, ZIFs' selectivity for CO_2 is more than double that of BPL carbon.

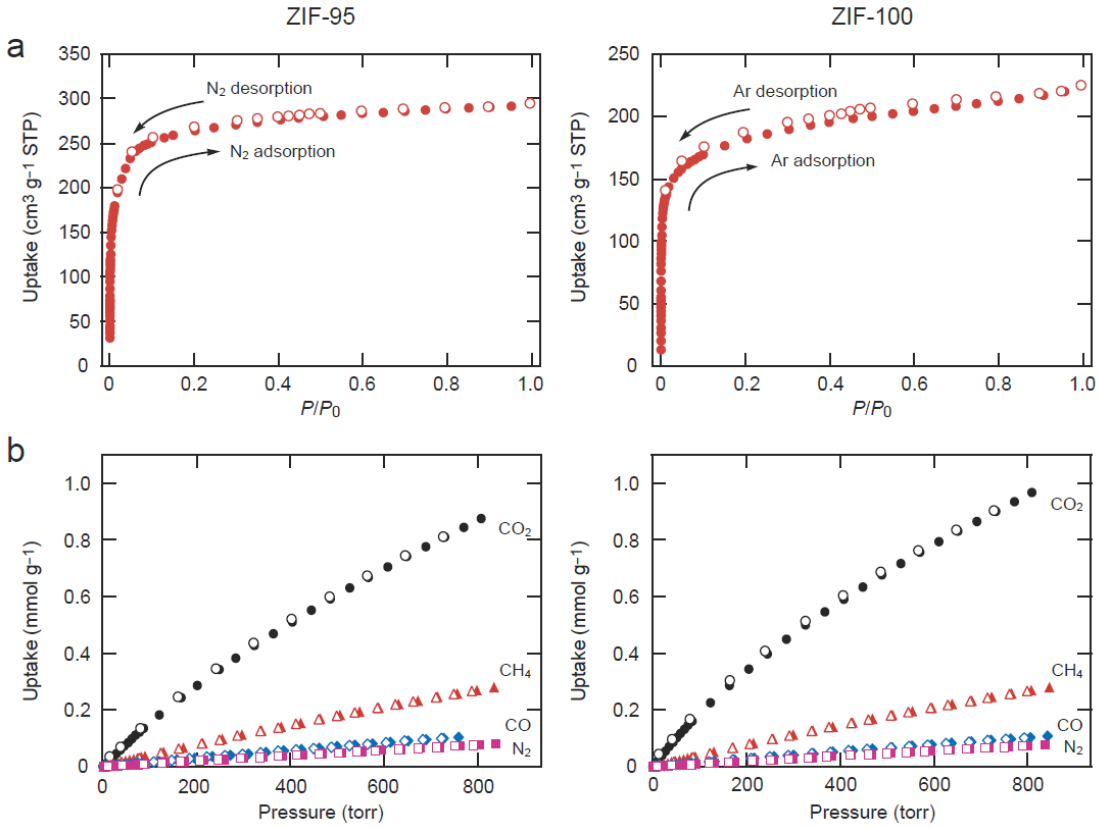

Figure 2. Gas adsorption isotherms of ZIF-95 (left) and ZIF-100 (right). (**a**) N_2 at 77 K for ZIF-95 (left); Ar at 87 K for ZIF-100 (right). (**b**) CO_2 (black, circles), CH_4 (red, triangles), CO (blue, diamonds) and N_2 (pink, rectangles) at 298 K for ZIF-95 (left) and ZIF-100 (right). The filled and open symbols represent adsorption and desorption branches, respectively.

Table 1. Calculated gas separation selectivity of ZIFs and BPL carbon

Material	Gas pairs	ZIFs Selectivity	BPL Carbon Selectivity [6]	Ratio ZIFs/BPL Carbon
ZIF-100	CO_2/CH_4	5.9 ± 0.4	2.5	2.4 ± 0.2
	CO_2/CO	17.3 ± 1.5	7.5	2.3 ± 0.2
	CO_2/N_2	25.0 ± 2.4	11.1	2.3 ± 0.2
ZIF-95	CO_2/CH_4	4.3 ± 0.4	2.5	1.7 ± 0.2
	CO_2/CO	11.4 ± 1.1	7.5	1.5 ± 0.1
	CO_2/N_2	18.0 ± 1.7	11.1	1.6 ± 0.2

2. Control of pore size and functionality in ZIFs

We have reported the synthesis of three new ZIFs, ZIF-68, 69, and 70, which are underlying the same GME topology but their functionalities are different [3]. We extended this concept to design other functionalized GME ZIFs. Specifically, we synthesized and characterized five new ZIFs, ZIF-78, 79, 80, 81, and 82 (Figure 3) [7].

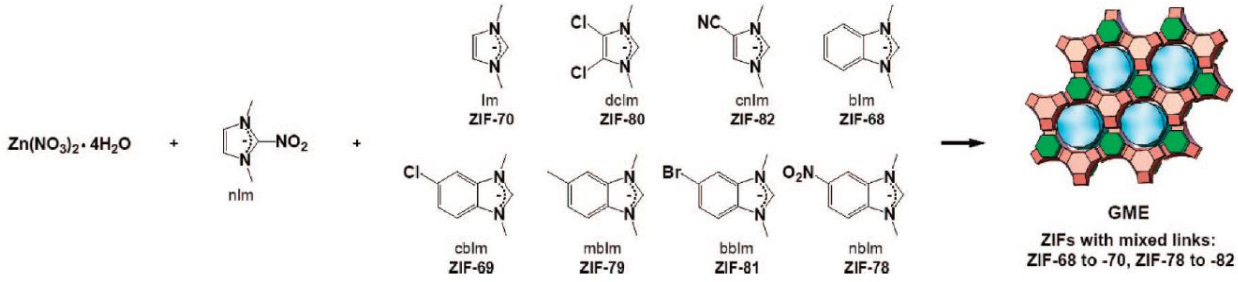

Figure 3. Structures of imidazolate links and their abbreviations. Reaction of nIm plus any other imidazole linker shown results in the **GME** topology, whose tiling is shown at the right. The name of the ZIF resulting from reaction with nIm is given under each linker.

The ZIFs reported here were synthesized solvothermally. The structures of ZIF-78 to 82, were determined from single-crystal X-ray diffraction data. In each ZIF, every tetrahedral Zn atom is connected to two 2-nitroimidazolate (nIm) and two other substituted Im (see Figure 3). Interestingly, across the series of Im linkers with -Cl, -CN, -Me, -Br, and -NO_2 functionality incorporated into the GME topology, the substituted Im's point into the voids of the *kno* cages (blue cage in Figure 3). Thus, by varying the substituted Im, one can systematically modulate the pore aperture of the *kno* cage from 3.8 to 13.1 Å and the pore diameter from 7.1 to 15.9 Å.

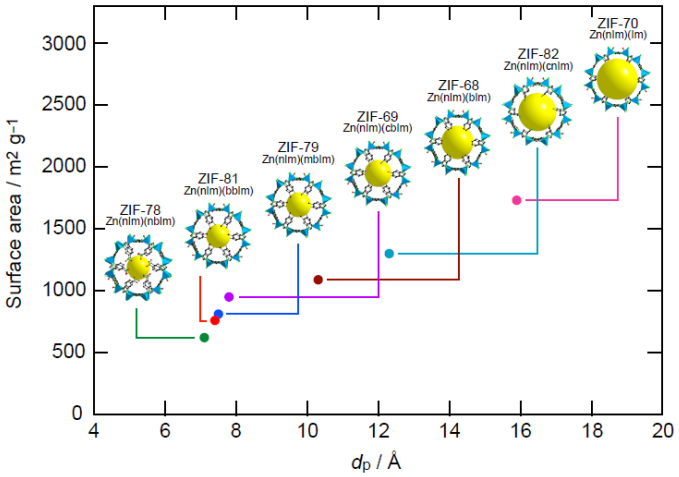

Figure 4. Plot of pore diameter (d_p) *vs.* surface area for the **GME** ZIFs, indicating a nearly linear relationship. To illustrate the variation of the pore size and functionality, the *kno* cage of each ZIF is shown. H atoms have been omitted for clarity. C, black; N, green; O, red; Cl, pink; Br, brown; Zn, blue tetrahedra.

Permanent porosity of the ZIFs was demonstrated by measuring the N_2 gas adsorption of the guest-free material. The BET surface areas for the seven ZIFs vary from 620 to 1730 m^2 g^{-1}. Figure 4 shows a nearly linear relationship between pore diameter and the specific surface area. This effect is likely the result of both reduced pore volume in the ZIFs with smaller pore dimensions and increased framework weight in the ZIFs bearing additional functional groups.

3. Postsynthesis covalent functionalization of ZIFs

In the previous section, we demonstrated the worth of reticular synthesis to introduce various functional groups without changing underlying topology. For the further development of this concept, we believe postsynthesis covalent functionalization of crystalline extended solids should also be pursued. Here, we implemented this strategy to ZIFs, which have unusual thermal and chemical stability, and thus are ideal platforms for performing useful organic transformations under strong reaction conditions [8]. Specifically, the imidazolate-2-carboxyaldehyde (ICA) links, which join tetrahedral zinc(II) centers in a new porous ZIF (vide infra), have been reduced by $NaBH_4$ to the corresponding alcohol derivative, and converted to an imine functionality in refluxing methanol (Figure 5).

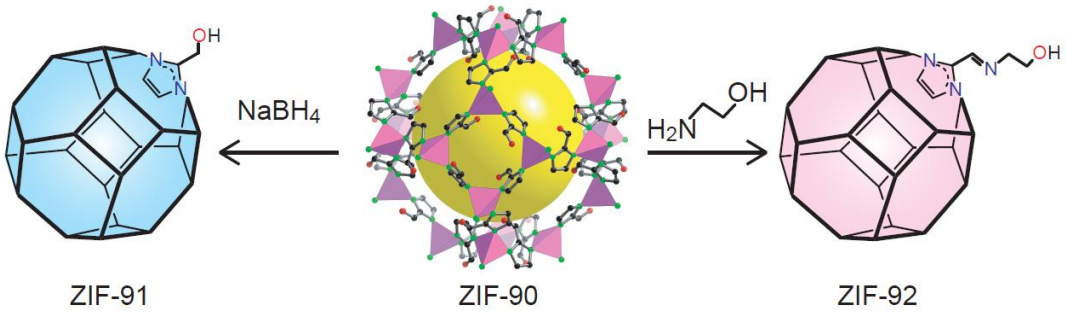

Figure 5. Transformation of ZIF-90 (center) by reduction with $NaBH_4$, and reaction with ethanolamine to give ZIF-91 (left) and ZIF-92 (right). Crystal structure of ZIF-90 presented as one of the ZIF cages with ZnN_4 tetrahedra in pink polyhedra and the ICA links in ball-and-stick representation (C, black; N, green; O, red). The yellow ball represents the largest sphere to fit in the porous cage without contacting the van der Waals spheres of the framework. H atoms have been omitted for clarity.

A new crystalline ZIF structure (termed ZIF-90, Figure 5) was synthesized by heating a solution mixture of H-ICA and $Zn(NO_3)_2$ in DMF at 100 °C for 18 h. The same material can also be obtained by diffusion of a triethylamine and hexane solution into a DMF mixture of H-ICA and $Zn(NO_3)_2$ at 25 °C for 24 h. Elemental analysis performed on guest free ZIF-90 gave the expected formula, $Zn(C_4H_3N_2O)_2$. Crystals of as-synthesized ZIF-90 where examined by single crystal X-ray diffraction (XRD) techniques and the structure was found to be related to the sodalite topology (SiO_2, **sod**) by replacing the Si and O with Zn(II) and ICA links, respectively. This leads to an expanded ZIF structure with large voids and an extended 3-D ZIF structure with an aperture of 3.5 Å in diameter and a pore size of 11.2 Å.

To perform the postsynthesis functionalization on crystals of ZIF-90, we first examined its porosity. The N_2 adsorption isotherm for the guest free ZIF-90 measured at 77 K (Figure 6A) showed a steep rise in the low-pressure region indicating the permanent porosity of the ZIF-90 framework. The calculated Langmuir and BET surface areas from the adsorption data for ZIF-90 were 1320 and 1270 $m^2 g^{-1}$, respectively.

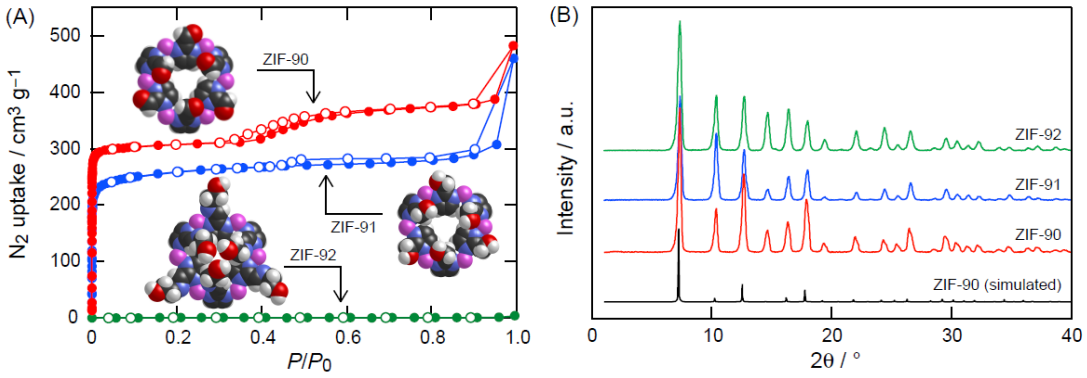

Figure 6. (A) N_2 isotherms of ZIF-90 (red), ZIF-91 (blue), and ZIF-92 (green) measured at 77 K. ZIF-90, 91, and 92 pore apertures are shown as space filled representations. (B) PXRD patterns of simulated ZIF-90 (black), ZIF-90 (red), ZIF-91 (blue), and ZIF-92 (green).

Reduction of aldehyde to alcohol functionality was achieved by reacting ZIF-90 with $NaBH_4$ in methanol at 60 °C for 24 h to give ZIF-91 (Figure 5). Remarkably, ZIF-91 maintained the high crystallinity of the parent framework (ZIF-90) as confirmed by their coincident PXRD patterns (Figure 6B). The presence of the alcohol group in ZIF-91 bulk samples was revealed by ^{13}C CP/MAS NMR spectroscopy. This showed the appearance of four imidazolate carbon atom resonances suggesting that two chemically distinct imidazolate links were present within the framework. Based on the NMR experiments of a digested sample of ZIF-91, it is presumed that approximately 80% conversion had been achieved. It is worthy to note that porosity of ZIF crystals was maintained throughout the conversion reaction of ZIF-90 to ZIF-91 (surface area of ZIF-91: 1070 and 1010 $m^2\ g^{-1}$ for Langmuir and BET surface areas, respectively, Figure 6A).

The chemical versatility of the aldehyde group was highlighted by performing another organic transformation on the ICA link of ZIF-90. Reaction of ZIF-90 with ethanolamine in methanol at 60 °C gave ZIF-92 (Figure 5). Quantitative conversion to the imine was completed within three hours as verified by ^{13}C CP/MAS NMR and FT-IR. As was the case for the conversion of ZIF-90 to ZIF-91, the high crystallinity of the ZIF structure was maintained as evidenced by the PXRD pattern of ZIF-92 (Figure 6B). The presence of the imine functionality in ZIF-92 severely constricts the pore aperture and prevents N_2 molecules from accessing the interior of the pores, as confirmed by its gas adsorption isotherm behavior (Figure 6A).

4. Isoreticular Metalation of MOFs

In the previous section, we demonstrated the covalent functionalization of ZIFs by carrying out organic reactions directly on ZIF crystals. Here we extended this strategy to implement the isoreticular metalation of extended crystalline materials [9]. In this study, we choose MOFs with large pores to be subjected to a sequence of chemical reactions to make a covalently bound chelating ligand. Specifically, crystals of $(Zn_4O)_3(BDC\text{-}NH_2)_3(BTB)_4$ (**A**) (Figure 7) were reacted with 2-pyridinecarboxaldehyde to form the covalently bound iminopyridine chelate derivative $(Zn_4O)_3(BDC\text{-}C_6H_5N_2)_3(BTB)_4$ (**B**), which was reacted with $PdCl_2(CH_3CN)_2$ to give the metal-complexed MOF $(Zn_4O)_3(BDC\text{-}C_6H_5N_2PdCl_2)_3(BTB)_4$ (**C**) [10,11].

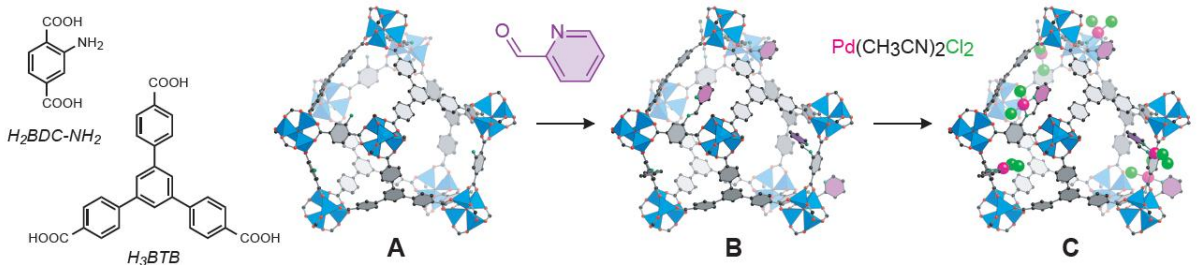

Figure 7. (Left) Molecular structures of organic links. (Right) Isoreticular covalent functionalization followed by metalation.

We sought to incorporate such a moiety into **A** through condensation of the amine-functionalized framework and 2-pyridinecarboxaldehyde (Figure 7). The isoreticular functionalized MOF **B** was synthesized by adding 2-pyridinecarboxaldehyde to **A** in anhydrous toluene and allowing the reaction to proceed for 5 days, during which the needle-shaped crystals changed color from clear to yellow to give a product having a composition that coincided well with the expected formula, thus indicating quantitative conversion. PXRD studies (Figure 8A) showed that **B** maintained crystallinity and possessed the same underlying topology as **A** subsequent to the covalent transformation. The presence of the iminopyridine unit was confirmed by mass spectrometry of digested samples of **B**.

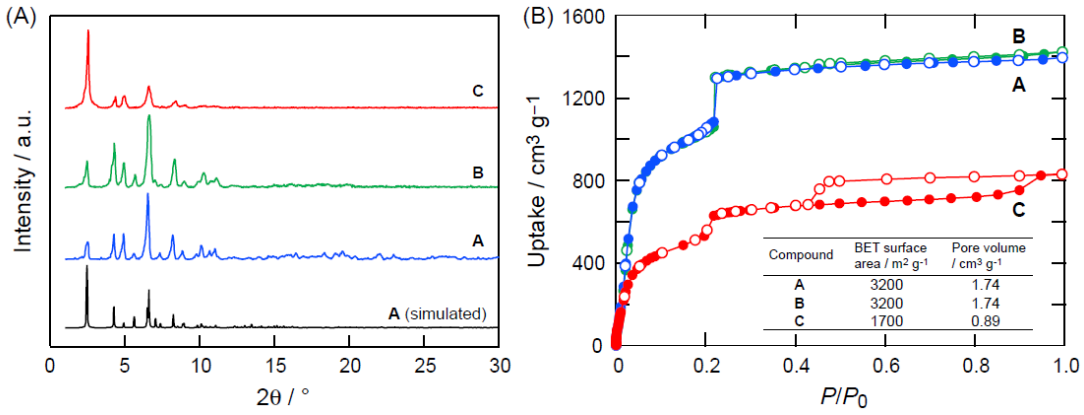

Figure 8. (A) PXRD patterns for **A** (blue), **B** (green), and **C** (red) along with a simulated pattern for **A** (black). (B) Ar gas adsorption isotherms for **A** (blue), **B** (green), and **C** (red) at 87 K, with adsorption and desorption points represented by solid and open circles, respectively.

Isoreticular metalation was achieved by adding $PdCl_2(CH_3CN)_2$ to **B** in anhydrous dichloromethane, whereupon the yellow crystalline material became dark-purple within several minutes. After 12 h, the material was washed with dichloromethane; the crystals were then immersed in dry dichloromethane for 3 days to yield **C**. Again, the PXRD pattern of **C** (Figure 8A) confirmed that it retained crystallinity and possessed a framework topology identical to those of **A** and **B**. Removal of guest species from the pores was achieved by evacuating the

crystals at 80 °C for 12 h. Elemental analysis performed on the guest-free framework of **C** gave a molecular formula $C_{50}H_{28}N_2O_{13}Zn_4PdCl_2$, whose Pd/Zn ratio of 1:4 is consistent with quantitative metalation of the iminopyridine sites.

The porosities of **B** and **C** were assessed by performing an 87 K Ar isotherm (Figure 8B). Notably, both materials maintained porosity after two subsequent chemical transformations. Additionally, analogous profiles were observed for **A**-**C**.

To confirm that the Pd is complexed to the iminopyridine unit and to precisely determine the Pd coordination environment within the framework, we performed Pd K-edge extended X-ray absorption fine structure (EXAFS) spectroscopy on samples of **C**. The data analysis indicated the presence of two Pd-Cl and two Pd-N ligands at 2.276(2) and 1.993(2) Å, respectively, and these Pd-N distances are consistent with crystallographic data (the Cambridge Structural Database) for analogous Pd compounds. Furthermore, analysis of the X-ray absorption near-edge structure (XANES) spectrum indicated that the major chemical form of Pd within the framework of **C** was consistent with an iminopyridine-bound moiety and not the starting material, $PdCl_2(CH_3CN)_2$.

5. Isoreticular expansion of MOFs with triangular and square building units

It is likely that larger pore is preferable for the metalation reaction, because the pore is not fully occupied by metal ions and their counter anions. The simplest way to expand the pore is to use longer organic linkers [12]. To this end, we performed the isoreticular expansion of MOFs using triangular organic linker and square inorganic secondary building units (SBUs, $Cu_2(CO_2)_4$) [13], because there are two famous MOF structures have been reported [14,15]. One is a MOF with the **tbo** topology in which Cu_2 square "paddlewheel" units are linked by benzenetricarboxylate (BTC) units has been known for some time and is known as HKUST-1 and/or MOF-199 [14]. Another is MOF-14 in which the same Cu_2 square "paddlewheel" units are linked by BTB units to produce a structure based on the **pto** topology [15].

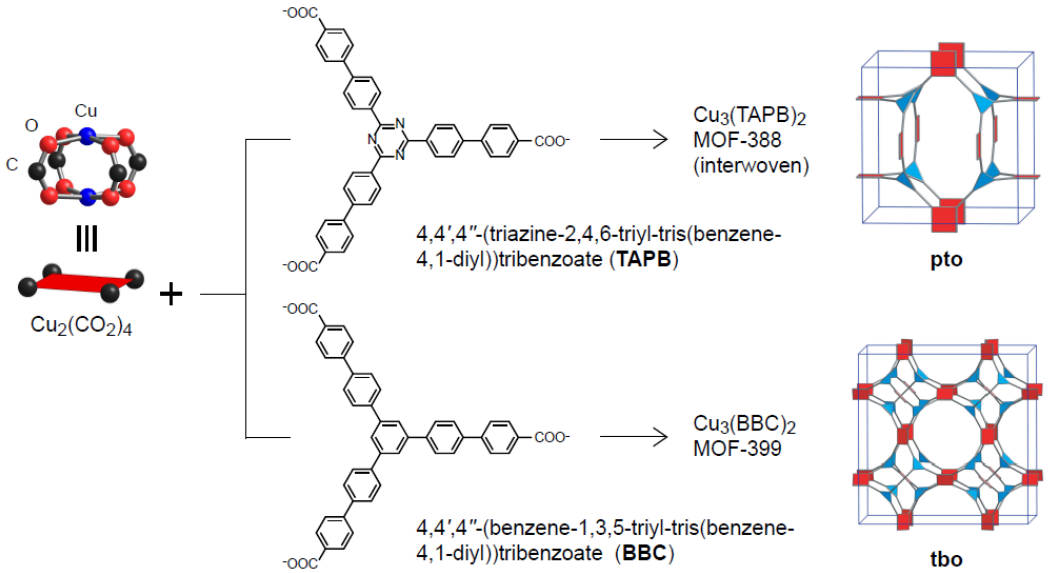

Figure 9. $Cu_2(CO_2)_4$ unit (Left) is connected with organic linkers (middle) to form MOFs. (right) **pto** and **tbo** nets shown in augmented form.

When we employed TAPB linker, an expanded **pto** net was also found with two interwoven nets (termed MOF-388, Figures 9 and 10). Blue hexahedron crystals of MOF-388 were obtained by a solvothermal reaction of H_3TAPB and $Cu(NO_3)_2 \cdot 2.5H_2O$ in a solvent mixture of DMF/NMP. Single crystal X-ray diffraction analysis revealed that Cu_2 paddlewheel square units are connected through tritopic TAPB linkers. The expansion from BTB to TAPB leads to the enlargement of the cage size in the single framework from 20.4 Å in MOF-14 to 27.1 Å in MOF-388. In spite of the interweaving, MOF-388 has a large cavity diameter (27.1 Å), void volume (84%) and crystal density (0.34 g cm^{-3}).

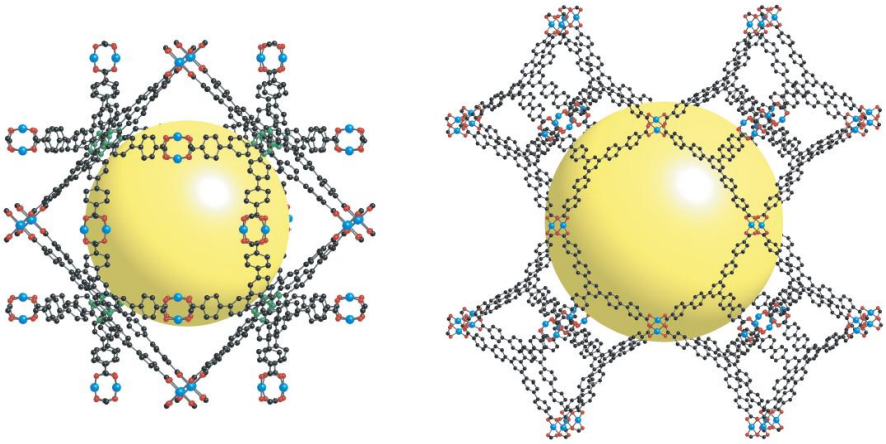

Figure 10. Single crystal structures of MOF-388 (left) and MOF-399 (right). The yellow ball is placed in the structure for clarity and to indicate space in the cage. Cu, blue; C, black; O, red; and N, green. Hydrogen atoms are omitted for clarity.

Crystals of MOF-399 were obtained by mixing a solution of BBC linker (Figure 9), whose structure is almost the same as TAPB except for the central benzene ring, with $Cu(NO_3)_2 \cdot 2.5H_2O$ in DMF/NMP. Its crystal structure is based on the **tbo** net; in contrast to MOF-388, the structure of MOF-399 (Figure 10) is isoreticular with HKUST-1 [14]. Expansion from BTC to BBC in this work led to greatly further enlargement of unit cell length from 26.34 Å in HKUST-1 to 68.31 Å in MOF-399, which corresponds to a volume expansion by a factor of 17.4 (Figure 10). The inner diameter of the cavity in MOF-399 measures 43.2 Å and has a largest ring comprised of 72 atoms. The density of MOF-399 with empty pores is the lowest yet reported, 0.126 g cm^{-3}, and it should be noted that this is even lower than that (0.17 g cm^{-3}) of COF-108 which is comprised of only light elements, C, H, B, and O [16].

6. Ultrahigh porosity in MOF-200 and 210.

In the previous section, we showed successful isoreticular expansion; though the surface areas of these materials were not high as expected. Considering the stability of inorganic SBUs, the octahedral $Zn_4O(CO_2)_6$, which are shown in MOF-5 and MOF-177 [17-19], can be better than Cu square unit ($Cu_4(CO_2)_4$). Therefore, the expanded forms of MOF-177 from BBC were prepared to give MOF-200, and used mixed BTE/BPDC links to obtain MOF-210 (Figures 11 and 12) [20].

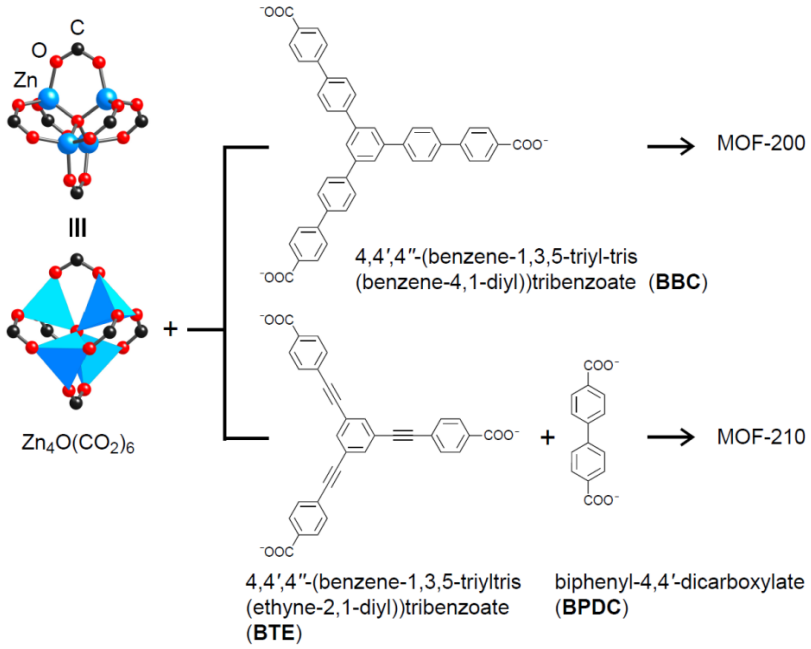

Figure 11. $Zn_4O(CO_2)_6$ unit (left) is connected with organic linkers (middle) to form MOFs.

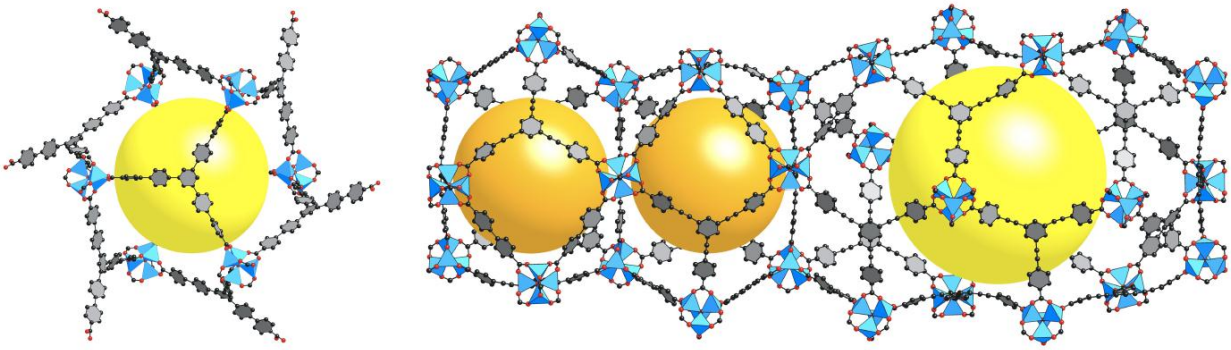

Figure 12. Single crystal structures of MOF-200 (left) and MOF-210 (right). Atom colors are the same as those in Figure 10.

MOF-200 and 210 were prepared from a solvothermal reaction of organic linkers and zinc nitrate, and the resulting crystals were characterized by single crystal X-ray diffraction. Considering the bulk density and void space calculated from the crystal structure analyses, MOF-200 and 210 are promising candidates to realize ultra-high surface area. However, preliminary trials revealed that the solvent exchange followed by pore evacuation under vacuum was not effective to activate MOF-200 and 210 without losing porosity. Therefore, these crystals were fully exchanged with liquid CO_2, kept under supercritical CO_2 atmosphere, followed by their pores being bled of CO_2 to yield activated samples. Successful guest removal was confirmed by PXRD measurements and elemental analyses [21].

As shown in Figure 12, these MOF samples show distinctive steps (P/P_0 = 0.14 and 0.27 for MOF-200 and 210), and the profiles for MOF-200 and 210 are nearly the same as the predicted isotherms by grand canonical Monte Carlo (GCMC) simulations (Prof. Snurr group (Northwestern Univ.)). The maximum N_2 uptake capacities at 77 K in MOF-200 and 210 are 2340 and 2330 cm^3 g^{-1}, respectively. More importantly, the measured values are near the values predicted based on the structure, indicating that these materials are well-activated. Because of the successful sample activation, extremely high BET (and Langmuir) surface areas were obtained: 4530 (10400) and 6240 (10400) m^2 g^{-1} for MOF-200 and 210. The BET surface area of MOF-210 was the highest reported for crystalline materials at the moment [22].

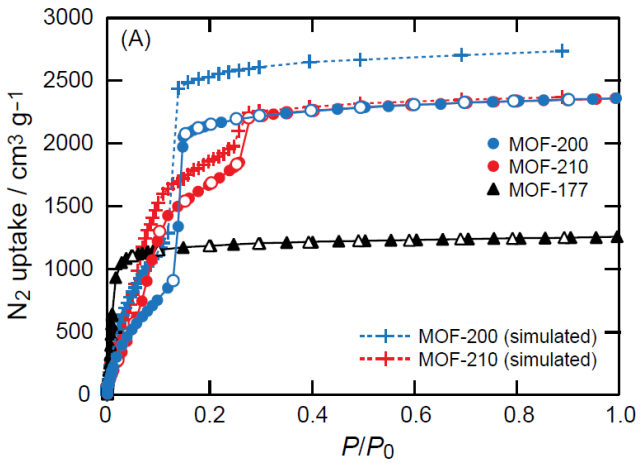

Figure 12. Low-pressure N_2 isotherms of MOF-177, 200, and 210 at 77 K. Simulated isotherms of MOF-200 and 210 were overlaid.

Concluding Remarks

The aim of this project is to develop the next generation of MOFs and ZIFs. By the systematic material design, synthesis, and characterization we demonstrated the effective strategies to introduce active functional groups in the frameworks, and this is also the origin of the new strategy, which is termed isoreticular functionalization and metalation. With that being said, a large pore volume is still a prerequisite feature. One of the solutions to overcome this challenge is isoreticular expansion of a MOF's structure. With triangular organic linkers and square building units, we demonstrated that MOF-399 has a unit cell volume 17 times larger than that of the first reported material isoreticular to it, while having the highest porosity (94%) and lowest density (0.126 g cm^{-3}) of any MOF reported to date. More importantly, MOFs are not just low density materials; the guest-free form of MOF-210 demonstrates ultrahigh porosity, whose BET surface area was estimated to be 6240 m^2 g^{-1} by N_2 adsorption measurements. In the future, further optimization of ZIFs and MOFs for gas separation is necessary, for example, tuning pore sizes and inclusion of various metals within the pores without losing porosity. We believe that the concept of the isoreticular expansion, functionalization, and metalation of porous MOFs and ZIFs demonstrated here would be powerful tools to meet the challenges and pursue practical gas separation media.

Publications Resulting from this Funding Period

1. Colossal Cages in Zeolitic Imidazolate Frameworks as Selective Carbon Dioxide Reserviors, B. Wang, A. P. Côté, H. Furukawa, M. O'Keeffe, and O. M. Yaghi, *Nature*, **2008**, *453*, 207-211.
2. Control of Vertex Geometry, Structure Dimensionality, Functionality, and Pore Metrics in the Reticular Synthesis of Crystalline Metal-Organic Frameworks and Polyhedra, H. Furukawa, J. Kim, N. W. Ockwig, M. O'Keeffe, and O. M. Yaghi, *J. Am. Chem. Soc.*, **2008**, *130*, 11650-11661.
3. Reticular Chemistry and Metal-Organic Frameworks for Clean Energy, O. M. Yaghi and Q. Li, *MRS Bulletin*, **2009**, 34, 682-690.
4. Synthesis, Structure, and Carbon Dioxide Capture Properties of Zeolitic Imidazolate Frameworks, Anh Phan, Christian Doonan, Fernando J. Uribe-Romo, Carolyn B. Knobler, Michael O'Keeffe, and Omar M. Yaghi, *Acc. Chem. Res*, **2009**, 43, 58-67.
5. Isoreticular Metalation of Metal-Organic Frameworks, C. J. Doonan, W. Morris, H. Furukawa, and O. M. Yaghi, *J. Am. Chem. Soc.*, **2009**, *131*, 9492-9493.
6. Control of Pore Size and Functionality in Isoreticular Zeolitic Imidazolate Frameworks and their Carbon Dioxide Selective Capture Properties, R. Banerjee, H. Furukawa, D. Britt, C. Knobler, M. O'Keeffe, O. M. Yaghi, *J. Am. Chem. Soc.*, **2009**, *131*, 3875-3877.
7. A Crystalline Imine-Linked 3-D Porous Covalent Organic Framework, F. J. Uribe-Romo, J. R. Hunt, H. Furukawa, C. Klock, M. O'Keeffe, O. M. Yaghi, *J. Am. Chem. Soc.*, **2009**, *131*, 4570-4571.
8. Storage of Hydrogen, Methane, and Carbon Dioxide in Highly Porous Covalent Organic Frameworks for Clean Energy Applications, H. Furukawa and O. M. Yaghi, *J. Am. Chem. Soc.*, **2009**, *131*, 8876-8883.
9. Highly efficient separation of carbon dioxide by a metal-organic framework replete with open metal sites, D. Britt, H. Furukawa, B. Wang, T. G. Glover, and O. M. Yaghi, *Proc. Natl. Acad. Sci. USA*, **2009**, 106, 20637-20640.
10. Multiple Functional Groups of Varying Ratios in Metal-Organic Frameworks, H. Deng, C. J. Doonan, H. Furukawa, R. B. Ferreira, J. Towne, C. B. Knobler, B. Wang, O. M. Yaghi, *Science*, **2010**, *327*, 846-850.
11. Exceptional Ammonia Uptake by a Covalent Organic Framework, C. J. Doonan, D. J. Tranchemontagne, T. G. Glover, J. R. Hunt, O. M. Yaghi, *Nature Chem.*, **2010**, *2*, 235-238.
12. A Metal-Organic Framework with Covalently Bound Organometallic Complexes, K. Oisaki, Q. Li, H. Furukawa, A. U. Czaja, O. M. Yaghi, *J. Am. Chem. Soc.*, **2010**, *132*, 9262-9264.
13. Ultra-High Porosity in Metal-Organic Frameworks, H. Furukawa, N. Ko, Y. B. Go, N. Aratani, S. B. Choi, E. Choi, A. O. Yazaydin, R. Q. Snurr, M. O'Keeffe, J. Kim, O. M. Yaghi, *Science*, **2010**, *239* 424 – 428.
14. Ring-Opening Reactions Within Metal-Organic Frameworks, D. Britt, C. Lee, F. J. Uribe-Romo, H. Furukawa, O. M. Yaghi, *Inorg. Chem.*, **2010**, *49*, 6387-6389.

15. Azulene Based Metal-Organic Frameworks for Strong Adsorption of H_2, S. Barman, H. Furukawa, O. Blacque, K. Venkatesan, O. M. Yaghi, H. Berke, *Chem. Commun.*, **2010**, *46*, 7981-7983.

16. Adsorption Mechanism and Uptake of Methane in Covalent Organic Frameworks: Theory and Experiment, J. L. Mendoza-Cortes, S. S. Han, H. Furukawa, O. M. Yaghi, W. A. Goddard III, *J. Phys. Chem. A.*, **2010**, *114*, 10824-10833.

17. Isoreticular Expansion of Metal-Organic Frameworks with Triangular and Square Building Units and the Lowest Calculated Density for Porous Crystals, H. Furukawa, J. Uribe-Romo, J. Kim, M. O'Keeffe, O. M. Yaghi, *Inorg. Chem.*, **2011**, *50*, 9147-9152.

18. Incorporation of Active Metal Sites in MOFs via *in situ* Generated Ligand Deficient Metal-Linker Complexes, S. Barman, H. Furukawa, O. Blacque, K. Venkatesan, O. M. Yaghi, G.-X. Jin, H. Berke, *Chem. Commun.*, **2011**, *47*, 11882-11884.

References

[1] K. S. Park, N. Zheng, A. P. Côté, J. Y. Choi, R. Huang, F. J. Uribe-Romo, H. K. Chae, M. O'Keeffe, O. M. Yaghi, *Proc. Natl. Acad. Sci. U.S.A.*, **2006**, *103*, 10186.

[2] H. Hayashi, A. P. Côté, H. Furukawa, M. O'Keeffe, O. M. Yaghi, *Nature Mater.*, **2007**, *6*, 501.

[3] R. Banerjee, A. Phan, B. Wang, C. Knobler, H. Furukawa, M. O'Keeffe, O. M. Yaghi, *Science*, **2008**, *319*, 939.

[4] A. Phan, C. J. Doonan, F. J. Uribe-Romo, C. B. Knobler, M. O'Keeffe, O. M. Yaghi, *Acc. Chem. Res.*, **2009**, 43, 58.

[5] B. Wang, A. P. Côté, H. Furukawa, M. O'Keeffe, O. M. Yaghi, *Nature*, **2008**, *453*, 207.

[6] S. Sircar, T. C. Golden, M. B. Rao, *Carbon*, **1996**, *34*, 1.

[7] R. Banerjee, H. Furukawa, D. Britt, C. Knobler, M. O'Keeffe, O. M. Yaghi, *J. Am. Chem. Soc.*, **2009**, *131*, 3875.

[8] W. Morris, C. J. Doonan, H. Furukawa, R. Banerjee, O. M. Yaghi, *J. Am. Chem. Soc.*, **2008**, *130*, 12626.

[9] C. J. Doonan, W. Morris, H. Furukawa, and O. M. Yaghi, *J. Am. Chem. Soc.*, **2009**, *131*, 9492.

[10] Z. Wang, K. K. Tanabe, S. M. Cohen, *Inorg. Chem.*, **2009**, *48*, 296.

[11] K. Koh, A. G. Wong-Foy, A. J. Matzger, *Angew. Chem. Int. Ed.*, **2008**, 47, 677.

[12] M. Eddaoudi, J. Kim, N. Rosi, D. Vodak, J. Wachter, M. O'Keeffe, O. M. Yaghi, *Science*, **2002**, *295*, 469.

[13] H. Furukawa, J. Uribe-Romo, J. Kim, M. O'Keeffe, O. M. Yaghi, *Inorg. Chem.*, **2011**, *50*, 9147.

[14] S. S.-Y. Chui, S. M.-F. Lo, J. P. H. Charmant, A. G. Orpen, I. D. Williams, *Science*, **1999**, *283*, 1148.

[15] B. Chen, M. Eddaoudi, S. T. Hyde, M. O'Keeffe, O. M. Yaghi, *Science*, **2001**, *291*, 1021.

[16] H. M. El-Kaderi, J. R. Hunt, J. L. Mendoza-Cortés, A. P. Côté, R. E. Taylor, M. O'Keeffe, O. M. Yaghi, *Science*, **2007**, *316*, 268.

[17] H. Li, M. Eddaoudi, M. O'Keeffe, O. M. Yaghi, *Nature*, **1999**, *402*, 276.

[18] N. L. Rosi, J. Eckert, M. Eddaoudi, D. T. Vodak, J. Kim, M. O'Keeffe, O. M. Yaghi, *Science*, **2003**, *300*, 1127.

[19] H. K. Chae, D. Y. Siberio-Pérez, J. Kim, Y. B. Go, M. Eddaoudi, A. J. Matzger, M. O'Keeffe, O. M. Yaghi, *Nature*, **2004**, *427*, 523.

[20] H. Furukawa, N. Ko, Y. B. Go, N. Aratani, S. B. Choi, E. Choi, A. Ö. Yazaydin, R. Q. Snurr, M. O'Keeffe, J. Kim, O. M. Yaghi, *Science*, **2010**, *239*, 424.

[21] A. P. Nelson, O. K. Farha, K. L. Mulfort, J. T. Hupp, *J. Am. Chem. Soc.*, **2009**, *131*, 458.

[22] O. K. Farha, I. Eryazici, N. C. Jeong, B. G. Hauser, C. E. Wilmer, A. A. Sarjeant, R. Q. Snurr, S.-B. T. Nguyen, A. Ö. Yazaydın, J. T. Hupp, *J. Am. Chem. Soc.*, **2012**, *134*, 15016.